ELSEVIER

Chemical Geology 182 (2002) 301–322

CHEMICAL GEOLOGY
INCLUDING
ISOTOPE GEOSCIENCE

www.elsevier.com/locate/chemgeo

Evidence for crustal components in the mantle and constraints on crustal recycling mechanisms: pyroxenite xenoliths from Hannuoba, North China

Yigang Xu *

Guangzhou Institute of Geochemistry, Chinese Academy of Sciences, P.O. Box 1131, Wushan, Guangzhou, 510640 China

Received 13 January 2000; accepted 26 April 2001

Abstract

Spinel and garnet pyroxenite xenoliths in Cenozoic basalts from Hannuoba, North China show extremely heterogeneous chemical and isotopic compositions ($\varepsilon_{Nd} = -27$ to $+34$). Most of these pyroxenites are relatively young, probably late Mesozoic in age, although a few Al-pyroxenites could be very old (~ 2 Ga). While their texture and major element compositions suggest an origin of high pressure cumulates, the trace element and isotopic compositions of the Hannuoba pyroxenites require multiple segregation processes from different parental magmas. Strong LREE enrichment, ubiquitous HFSE depletion and some Eu anomalies of the Al- and Cr-pyroxenites indicate the involvement of crust components in their source. Their Sr–Nd isotopic ratios are negatively correlated and plot below the MORB–OIB–IAB–sediment trend, suggesting that the parental melts of the Cr- and Al-pyroxenites may have been derived from a mixture of asthenospheric melts and a long-term evolved continental crust. The garnet pyroxenites significantly deviate from the isotopic array defined by the Al-pyroxenites, due to their relatively high $^{87}Sr/^{86}Sr$ at given ε_{Nd}. They thus more likely represent segregates from melts derived from partial melting of hydrothermally altered oceanic crust (basalts + marine sediment). If the crustal component involved in the Al-pyroxenites is subducted terrigenous sediments or other continental materials from the Archean Sino-Korean Craton, the Al-pyroxenites and garnet pyroxenites may have formed contemporaneously at a palaeo-convergent plate margin. This may be related to the subduction of the Mongol–Okhotsk plate beneath North China during the late Jurassic. Alternatively, if the delaminated lower crust was involved, it implies that most of the Al-pyroxenites are younger than the garnet pyroxenites, and their formation may be temporally correlated with lithospheric thinning during the Cretaceous. This model is attractive because the inferred tectonic evolution from a convergent setting to an extensional environment is consistent with the geologic record in the area.

Keywords: Pyroxenite xenoliths; Trace element; Isotope; Crustal recycling; Hannuoba

1. Introduction

It is generally accepted that most pyroxenites are derived by high pressure crystal-segregation from melts flowing through conduits in the mantle, as a result of temperature difference between ascending

* Tel.: +86-20-85290109; fax: +86-20-85290130.
E-mail address: yigangxu@gig.ac.cn (Y. Xu).

0009-2541/02/$ - see front matter
PII: S0009-2541(01)00300-X

melt and their peridotitic wall-rocks (Irving, 1980; Bodinier et al., 1987; Suen and Frey, 1987). Asthenosphere, enriched continental lithospheric mantle or subducted, metamorphosed oceanic lithosphere and its deviates have been proposed as sources of parental magmas to pyroxenites (Griffin et al., 1988; Medaris et al., 1995; Pearson et al., 1993; Becker, 1996). However, there is increasing evidence for more complex genesis for some pyroxenites, involving direct solid-state recycling of subducted lithosphere (Allegre and Turcotte, 1986), partial melting (Loubet and Allegre, 1980) and melt-rock reactions at decreasing melt mass along near-solidus isotherms (Garrido and Bodinier, 1999). Pyroxenite xenoliths are also the physical manifestation of mantle heterogeneity. The migration of their parental magmas and derivative fluids in the lithospheric mantle is considered an important mechanism of mantle metasomatism (Menzies et al., 1985; Griffin et al., 1988; Bodinier et al., 1990). On the other hand, because of their lower solidus temperature compared with peridotites, pyroxenites may significantly contribute to partial melting during pressure release of the adiabatic mantle or thermal erosion of the lithospheric mantle. Accordingly, geochemical characterization of pyroxenites is helpful for understanding of metasomatic processes, recycling of crustal components in the mantle and the origin of intra-plate volcanism.

Recent petrologic and geochemical investigations in China have been mainly conducted on peridotite xenoliths (Song and Frey, 1989; Tatsumoto et al., 1992; Qi et al., 1995; Xu et al., 1996b, 1998). Pyroxenites have also been examined but principally for geothermobarometric purposes (Xu et al., 1996a, 1999). Preliminary isotopic data (Tatsumoto et al., 1992; Chen et al., 1997; Zhang et al., 1998b), however, show that pyroxenites from China have extremely variable isotopic compositions ($^{87}Sr/^{86}Sr$ up to 0.710 and $^{143}Nd/^{144}Nd$ down to 0.5114), which are significantly different from those of the host basalts. They also contrast sharply with peridotites, which reveal an overall depleted mantle signature for the subcontinental mantle beneath eastern China. Therefore, these pyroxenites provide direct evidence for enriched components in the Chinese mantle. Alternatively, they could be relicts of old metasomatized lithospheric mantle, most of which was delaminated in the late Mesozoic (Griffin et al., 1998; Xu, 2001). Despite their potential importance for the understanding of mantle processes and regional geodynamics, a systematic study of the Chinese pyroxenites is not available.

In this contribution, major elements, rare earth (REE) and trace element and Sr–Nd isotopic data for a suite of pyroxenite xenoliths from Hannuoba, North China, are presented. These data are used to place petrogenetic constraints on the origin of diverse pyroxenites and to characterize recycled crustal components in the mantle under the Sino-Korean Craton. Furthermore, the mechanism by which crustal components are recycled to the mantle and the role of pyroxenites in intraplate basaltic genesis and in mantle metasomatism will be evaluated.

2. Geological setting and petrography of pyroxenite xenoliths

Hannuoba is a classic xenolith locality in eastern China. It lies within the Sino-Korean Craton which underlies an area ca. 3000 km long (E–W) and up to 1500 km across (Fig. 1a). The basement rocks of the Sino-Korean Craton are Archean to early Proterozoic gneisses of amphibolite to granulite facies, with radiometric ages ranging from 2500–3800 Ma (Jahn et al., 1987). Two large-scale major geological and geophysical linear zones cut cross the Sino-Korean Craton. To the east, the craton is cut by the Tan–Lu Fault Zone (TLFZ) which is associated with significant Cenozoic and Mesozoic volcanism. To the west, the craton is traversed by the N–S trend Daxinganling–Taihangshan gravity lineament (DTGL). It is recognized that this zone separated two fundamentally different tectonic domains (Ma, 1989). The region to the west of this gravity zone is characterized by thick crust (>40 km), large negative Bouguer gravity anomalies, low heat flow and a thick (>150 km) lithosphere (Fig. 1). In contrast, to the east, the crust is thin (<35 km), the regional Bouguer gravity anomaly is weakly negative to positive, heat flow is high and lithosphere is inferred to be thin (Chen et al., 1991).

The Hannuoba basaltic plateau is located to the western side of the DTGL (Fig. 1). It covers an area of 1700 km^2 with lava thickness varying from 100 to over 500 m. The lower part of lava sequence is

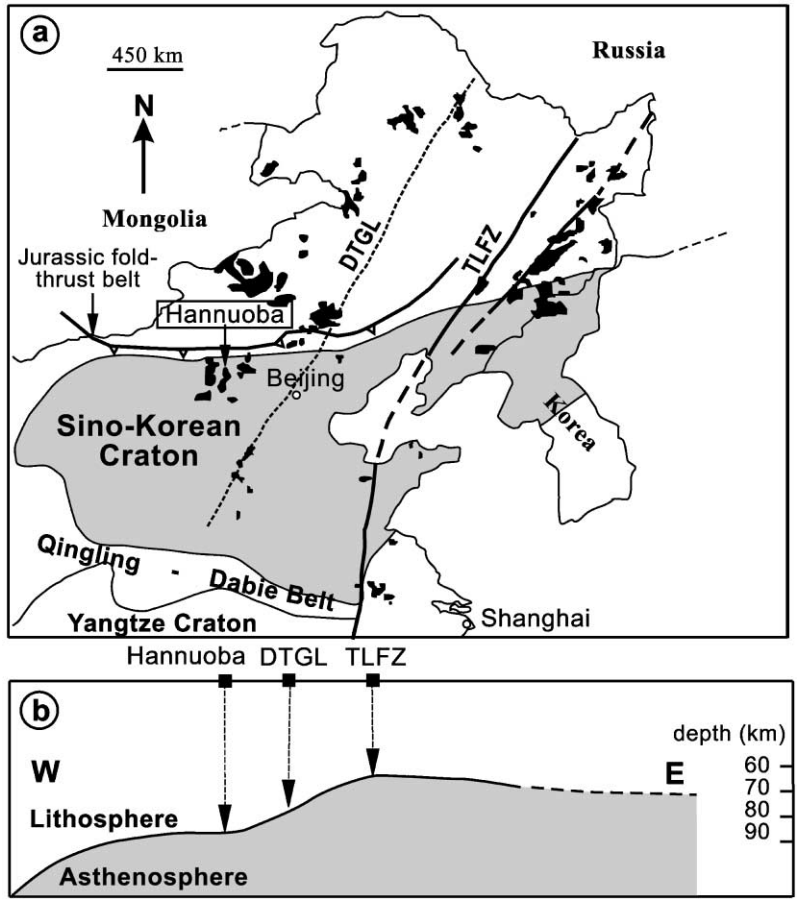

Fig. 1. (a) A sketch map showing the distribution of Hannuoba basalts and regional tectonic framework (modified after Xu et al., 1998). Note that the Archean Sino-Korean Craton is cut by two major geological and geophysical linear zones—Tan–Lu fault zone (TLFZ) to the east and Daxinganlin–Taihang gravity lineament (DTGL) to the west. Along the northern boundary of the Sino-Korean Craton, there is a late Jurassic E–W-trending fold-and-thrust belt (Yin and Nie, 1996). The Hannuoba locality is situated at the western side of the DTGL and not far from the fold-and-thrust belt. (b) Variation of thickness of the lithosphere across eastern China (after Chen et al., 1991).

mainly composed of alkali basalts of early Miocene age (Zhi et al., 1990). In the middle and upper sections (middle Miocene), the rocks are interlayered alkali basalt and tholeiite with tholeiites becoming dominant (Zhi et al., 1990). Along the southern edge of the Hannuoba basaltic field, there are more than forty localities where extremely abundant xenoliths have been found in alkali basalts. The dominant xenoliths are spinel peridotites which have been the subject of a few geochemical studies (Song and Frey, 1989; Tatsumoto et al., 1992). Subordinate pyroxenites and granulites are also present. The xenoliths investigated in this study were collected from Damaping, Xiaomaping and Jieshaba. They are divided into three groups following the classification of Whilshire and Shervais (1975): (1) Al-augite pyroxenites, which are either spinel-bearing or spinel-free (Al-pyroxenites); (2) Cr-diopside spinel pyroxenites (Cr-pyroxenites); and (3) garnet pyroxenites.

The Al-augite pyroxenite group includes clinopyroxenite and websterite. They occur either as veins in composites or as discrete nodules. The cross-cutting relationships between these pyroxenites and peridotites observed in composite xenoliths suggest a magmatic origin of the Al-pyroxenites. This is consistent with the cumulate textures in some samples.

However, most samples in this group are characterized by reequilibration microstructure with granoblastic being the most common. They are fine- to medium-grained (1–2 mm). Clinopyroxene is the dominant phase, but orthopyroxene, spinel and in some cases rare olivine are also present. Hydrous minerals are generally absent, but rare phlogopite has been documented by Tatsumoto et al. (1992). Application of the two-pyroxene thermometer of Bertand and Mercier (1986) yields higher equilibration temperatures (850–950°C) for spinel pyroxenites than for the spinel-free pyroxenites (< 850°C, Xu et al., in preparation).

The rock type of the Cr-pyroxenites includes clinopyroxenite, opx-rich websterite and orthopyroxenites. The opx-rich pyroxenites have relatively coarse grain size (6–8 mm), whereas Cr-clinopyroxenites are fine to medium grained with minor olivine. The later has cumulate or partially re-equilibrated texture, with exsolution of orthopyroxene lamella in clinopyroxene. Composites of Cr-pyroxenite and peridotite are abundant.

The garnet pyroxenites comprise websterite and clinopyroxenite. They have a granoblastic texture with a coarser grain size (> 4 mm) than the Al-pyroxenites. Pink garnet shows some retrograded feature. Composites of garnet pyroxenite–peridotite are not found in our collection, but were documented by Fan et al. (2001). Some garnet pyroxenites show clear modal layering. Most garnet pyroxenites equilibrated at 900–1106°C and 14–21 kbar (using the two-pyroxene thermometer of Bertand and Mercier, 1986 and garnet-orthopyroxene barometer of Nickel and Green, 1985).

3. Analytical methods

The pyroxenite xenoliths were sawn into slabs and central parts of more than 200 g were cleaned with distilled water in ultrasonic bath for 30 min. The rocks were then crushed in a steel mortar and grounded in a carbide mill. The bulk major element compositions were obtained using conventional wet chemistry at the Guangzhou Institute of Geochemistry. The rocks have also been analyzed for 35 trace elements (including REE) abundances using an Inductively Coupled Plasma-Mass spectrometer (ICP-MS) at the same institute. Analytical procedure was described by Liu et al. (1996). The powders (~ 50 mg) were dissolved in distilled HF-HNO_3 in Savillex screwtop Telfon breakers at 150°C for > 4 days. Precision for REE and HFSE is estimated to be 5% from repeatedly analyzed USGS standards BHVO-1 (basalt) and W-2 (diabase). The measured values of international standards are in satisfactory agreement with the recommended values (Table 1). Analyses of the internal standard RO-A1 (pyroxenite, provided by Dr. J.-L. Bodinier, Montpellier) at Guangzhou and Montpellier yield generally similar results (Table 1).

Isotopic ratios of Sr and Nd and elemental concentrations for Rb, Sr, Sm and Nd have been measured by isotope dilution on a subset of whole rock powder. Sample preparation and column chemistry are similar to those described by Jahn et al. (1980). The isotopic analyses were performed on a Finnigan MAT-261 multi-collector mass spectrometer at the Institute of Geology, Chinese Academy of Geological Sciences, Beijing. Analyses of standards during the period of analysis are as follows: NBS987 gave $^{87}Sr/^{86}Sr = 0.71025 \pm 2$ (2 S.D.); BCR-1 gave $^{143}Nd/^{144}Nd = 0.512643 \pm 12$ (2 S.D.). The blanks of Nd and Sr are 0.05 and 0.1–1 ng, respectively.

4. Analytical results

4.1. Major and minor elements

Major element abundance for pyroxenites is given in Table 2 and illustrated in Fig. 2. Published pyroxenite data in Chinese literature are also included for completeness and peridotite data are shown for comparison. As shown in Fig. 2, each petrographic group exhibits a wide range in composition that largely reflects variation in modal abundance of minerals and fractionation. For example, opx-rich pyroxenites display lower CaO and Al_2O_3 contents than cpx-rich samples. Despite some overlaps and exceptions, it can be generalized that the Al-pyroxenites are compositionally transitional between the Cr-pyroxenites and the garnet pyroxenites (Fig. 2). Cr-pyroxenites commonly have higher Mg# values (0.88–0.92) than

Table 1
Measured data for minor and trace elements in international reference materials (BHVO-1, W-2) and internal standard (RO-A1) (ppm)
Reference data for BHVO-1 and W-2 are taken from Govindaraju (1989).
Reference data for RO-A1 is the average of 28 analyses made at Montpellier (compiled by Remaidi, 1993).

	BHVO-1		W-2		RO-A1	
	This work ($n = 30$)	Reference	This work ($n = 23$)	Reference	This work ($n = 6$)	Reference
P	1166 ± 51	1201	541 ± 91	576		
Cr	275 ± 12	289	88.2 ± 0.4	93	1758 ± 266	
Mn	1295 ± 9	1293	1260 ± 12	1255	1223 ± 115	
Co	44.7 ± 0.4	45.0	44.3 ± 0.2	44.0	65 ± 4	
Ni	121.2 ± 1.8	120.0	74.2 ± 0.9	70.0	1070 ± 43	
Cu	137.7 ± 1.0	136.0	102.7 ± 1.4	103.0	59 ± 8	
Ga	24.7 ± 0.4	21.0	20.4 ± 0.3	20.0	9.1 ± 0.7	
Zn	106.3 ± 2.4	105.0	76.9 ± 2.9	77.0	51 ± 16	
Sc	31.7 ± 0.4	31.8	37.1 ± 2.4	35.0	26.2 ± 3.5	
Ti	16787 ± 598	16610	6116 ± 306	6360	4444 ± 166	
V	317.5 ± 3.4	317.0	259.7 ± 3.4	262.0	183 ± 10	195 ± 5
Rb	9.8 ± 0.5	11.0	30.3 ± 0.3	20.0	0.63 ± 0.11	0.68 ± 0.06
Sr	395.3 ± 11.9	403.0	201.6 ± 5.4	194.0	37.6 ± 2.0	36.3 ± 1.9
Y	28.0 ± 0.2	28.0	22.2 ± 0.1	23.0	14.8 ± 1.2	
Zr	176.3 ± 5.6	179.0	93.3 ± 1.3	94.0	38.6 ± 4.0	35.0 ± 3.0
Nb	19.2 ± 0.2	19.5	7.3 ± 0.1	7.8	0.08 ± 0.01	0.09 ± 0.02
Ba	139.1 ± 5.1	139.0	173.9 ± 6.6	173.0	1.49 ± 0.42	1.20 ± 0.20
Hf	4.58 ± 2.4	4.38	2.47 ± 0.16	2.40	1.24 ± 0.09	1.25 ± 0.10
Ta	1.18 ± 0.01	1.23	0.44 ± 0.02	0.50	0.027 ± 0.003	0.016 ± 0.002
Th	1.27 ± 0.04	1.25	2.18 ± 0.07	2.20	0.014 ± 0.006	0.009 ± 0.002
U	0.43 ± 0.02	0.42	0.50 ± 0.01	0.53	0.007 ± 0.007	0.0035 ± 0.0014
La	15.16 ± 0.38	15.80	10.15 ± 0.20	10.00	1.09 ± 0.16	1.12 ± 0.10
Ce	37.13 ± 0.84	39.00	22.54 ± 0.33	23.50	4.25 ± 0.15	4.25 ± 0.19
Pr	5.64 ± 0.16	5.45	3.03 ± 0.11	3.20	0.82 ± 0.05	0.83 ± 0.04
Nd	25.90 ± 0.81	25.20	13.39 ± 0.30	14.00	4.66 ± 0.26	4.65 ± 0.18
Sm	6.26 ± 0.16	6.17	3.23 ± 0.09	3.25	1.63 ± 0.09	1.59 ± 0.08
Eu	2.04 ± 0.05	2.06	1.06 ± 0.02	1.01	0.60 ± 0.03	0.60 ± 0.03
Gd	6.35 ± 0.30	6.22	3.60 ± 0.14	3.60	2.21 ± 0.15	2.16 ± 0.09
Tb	0.99 ± 0.03	0.95	0.61 ± 0.02	0.63	0.40 ± 0.02	0.38 ± 0.02
Dy	5.25 ± 0.13	5.25	3.67 ± 0.19	3.80	2.49 ± 0.15	2.48 ± 0.11
Ho	0.96 ± 0.02	1.00	0.75 ± 0.03	0.76	0.53 ± 0.04	0.52 ± 0.03
Er	2.37 ± 0.01	2.56	2.03 ± 0.07	2.40	1.45 ± 0.08	1.48 ± 0.07
Tm	0.34 ± 0.01	0.33	0.31 ± 0.00	0.38	0.22 ± 0.02	0.21 ± 0.01
Yb	2.00 ± 0.02	2.02	1.97 ± 0.08	2.05	1.38 ± 0.03	1.35 ± 0.07
Lu	0.30 ± 0.02	0.29	0.31 ± 0.02	0.33	0.22 ± 0.02	0.22 ± 0.01

the Al-augite group (0.74–0.89). The garnet pyroxenites overlap in composition with the Al-pyroxenites but trend towards even lower Mg# (0.63–0.86). The Hannuoba pyroxenites show considerable scatters in major oxide variation diagrams and do not plot along the inter-element correlation defined by fertile and residual peridotites (Fig. 2). There is a positive correlation between Cr and Ni and MgO in pyroxenites. The overall range of Ni abundance is very large (25–1773 ppm) with the lowest Ni contents in garnet pyroxenites. Similar to observations by Suen and Frey (1987) and Pearson et al. (1993), incompatible elements such as Zr, Sm and Sr show no correlation with Mg#.

4.2. Trace elements

In accordance with their lithological heterogeneity, the Hannuoba pyroxenites exhibit substantial

Table 2
Whole rock major and trace element concentrations of pyroxenites from Hannuoba

	Al-pyroxenites								Cr-pyroxenites				Garnet pyroxenites			
	H-1	H-2	H-3	H-4	H-8	H-9	H-12	H-13	H-5	H-7	H-11	H-14	97jsb-2	97jsb-6	97jsb-22	97xmp-1
SiO_2	48.80	49.63	50.18	49.37	46.55	50.04	50.64	51.50	50.15	47.37	52.37	54.68	47.24	47.87	48.05	45.6
TiO_2	0.42	0.21	0.40	0.21	0.13	0.30	0.20	0.32	0.20	0.18	0.30	0.11	0.66	0.40	0.67	0.55
Al_2O_3	6.08	7.86	5.40	7.80	4.03	6.69	7.02	6.93	6.83	5.71	6.37	3.72	10.28	9.43	9.37	8.79
Fe_2O_3	2.52	0.94	2.02	1.26	1.17	1.00	0.85	2.47	1.05	0.40	1.55	1.54	3.79	2.06	2.88	7.30
FeO	8.87	4.51	9.65	2.75	6.74	5.54	6.15	4.47	3.09	3.84	5.14	3.95	6.14	5.90	7.58	4.62
MnO	0.20	0.14	0.24	0.08	0.15	0.15	0.22	0.14	0.11	0.11	0.15	0.11	0.14	0.12	0.12	0.12
MgO	19.89	22.05	18.91	13.74	31.19	21.97	18.43	23.72	19.84	24.50	29.92	33.41	20.35	20.3	19.52	13.61
CaO	11.62	12.05	11.41	22.72	7.69	12.39	14.71	8.60	15.70	14.18	2.70	1.64	8.87	10.29	7.74	14.92
Na_2O	0.81	0.95	1.05	1.32	0.56	0.88	0.87	0.61	1.29	1.01	0.62	0.48	1.07	0.94	1.26	1.12
K_2O	0.02	0.31	0.03	0.03	0.03	0.03	0.13	0.19	0.03	0.15	0.04	0.02	0.37	0.32	0.40	0.29
P_2O_5	0.03	0.04	0.03	0.03	0.03	0.04	0.03	0.04	0.06	0.34	0.05	0.04	0.1	0.08	0.13	0.11
H_2O+	0.88	1.38	0.80	0.43	1.23	0.90	0.89	0.81	1.17	1.81	0.58	0.66	1.35	2.10	1.96	2.59
Total	100.14	100.07	100.12	99.74	99.50	99.93	100.14	99.80	99.52	99.60	99.79	100.36	100.4	99.81	99.68	99.62
Mg#	0.76	0.88	0.75	0.87	0.88	0.86	0.83	0.87	0.90	0.91	0.89	0.92	0.79	0.82	0.77	0.68
Trace elements contents (ppm)																
P	45.4	111.6	68.5	38.2	18.2	74.6	31.5	96.4	126.1	1462	68.8	17.6	336	162	405	220
Cr	1085	2299	1451	15	2235	2693	1147	1467	8380	4749	2974	3928	2457	2598	1565	1687
Mn	1381	1058	1691	619	1077	1048	1530	1034	825	717	1065	882	1455	1279	1267	1322
Co	83.8	55.2	71.8	13.7	110.6	60.0	60.0	67.2	42.4	54.7	64.6	63.2	51.8	49.0	57.8	74.3
Ni	435	1153	411	25	1773	767	397	1409	589	1101	757	1239	735	640	650	620
Cu	105.3	142.2	32.0	2.3	222.4	157.0	86.6	221.2	49.1	74.7	17.0	8.2	78.1	41.7	51.9	116.4
Ga	9.6	7.8	11.5	11.9	3.7	7.0	8.6	9.0	5.6	3.5	6.5	3.5	9.44	7.97	10.47	9.77
Zn	80.5	26.1	144.0	61.5	50.0	32.7	27.2	41.9	28.2	27.2	37.5	32.9	33.57	25.59	48.91	38.36
Sc	34.5	30.1	46.2	3.7	30.0	35.4	56.5	21.9	30.8	31.3	15.2	11.6	27.70	40.64	26.07	48.81

Ti	3632	2089	2847	1802	1071	2103	1538	3425	1039	1398	2309	596	1.98	1.79	1.78	2.28
V	199.9	219.0	231.3	47.5	106.8	191.2	305.7	162.2	145.2	181.1	123.2	66.0	3955	2250	3758	3380
Rb	0.34	9.72	0.51	0.08	0.58	0.34	5.27	5.06	0.42	4.73	0.82	0.24	192	206	179	285
Sr	106.5	71.5	43.3	196.6	23.3	56.1	86.5	45.0	123.7	207.9	17.3	6.5	9.09	11.64	5.66	11.62
Y	8.22	8.84	13.37	7.96	2.93	5.69	8.16	13.02	5.15	6.95	2.76	1.05	175	128	175	196
Zr	15.81	10.75	55.22	99.38	4.59	11.74	4.59	22.48	21.80	7.44	10.44	3.23	20.69	15.64	14.06	9.08
Nb	0.50	1.61	1.39	2.14	0.20	1.13	0.71	1.85	2.96	2.95	1.27	0.89	46.40	22.12	43.45	24.83
Ba	1.00	43.51	3.91	1.89	0.54	1.01	79.83	29.03	1.27	30.93	4.83	0.14	6.27	2.61	7.66	5.41
Hf	0.69	0.40	1.41	3.36	0.18	0.38	0.20	0.76	0.32	0.32	0.33	0.09	62.55	45.99	61.78	76.85
Ta	0.01	0.11	0.08	0.38	0.02	0.06	0.05	0.13	0.41	0.17	0.08	0.08	1.57	0.87	1.47	0.83
Th	0.04	0.14	0.09	0.68	0.02	0.10	0.08	0.16	0.46	1.25	0.08	0.13	0.74	0.34	1.03	1.09
U	0.11	0.08	0.09	0.18	0.02	0.08	0.06	0.08	0.16	0.39	0.06	0.05	0.23	0.14	0.24	0.27
La	1.47	1.16	9.08	5.94	0.32	1.02	0.58	1.14	5.75	13.04	0.87	0.63	4.29	1.80	5.40	4.50
Ce	5.60	2.69	32.33	19.73	1.07	2.98	1.19	2.75	14.15	24.61	2.10	1.04	9.66	4.07	11.16	9.36
Pr	1.13	0.41	5.10	3.14	0.20	0.54	0.18	0.45	1.85	2.58	0.30	0.11	1.30	0.59	1.47	1.22
Nd	6.29	2.15	21.69	13.46	1.18	2.94	1.00	2.51	7.16	8.97	1.44	0.35	6.42	3.14	6.96	5.79
Sm	1.90	0.78	4.47	2.68	0.41	0.92	0.54	1.05	1.18	1.45	0.39	0.08	1.90	1.13	1.88	1.44
Eu	0.66	0.33	0.99	0.73	0.16	0.37	0.29	0.42	0.39	0.50	0.14	0.03	0.65	0.42	0.62	0.59
Gd	2.08	1.27	3.83	2.16	0.55	1.12	1.15	1.83	0.99	1.51	0.49	0.11	2.39	1.55	2.05	1.51
Tb	0.31	0.24	0.53	0.31	0.09	0.18	0.21	0.35	0.16	0.24	0.08	0.02	0.47	0.32	0.37	0.25
Dy	1.79	1.62	2.82	1.57	0.57	1.13	1.55	2.41	0.98	1.38	0.52	0.15	3.29	2.38	2.31	1.51
Ho	0.35	0.36	0.54	0.30	0.13	0.23	0.34	0.53	0.20	0.29	0.11	0.04	0.80	0.61	0.54	0.30
Er	0.92	1.04	1.48	0.84	0.35	0.65	0.94	1.48	0.61	0.80	0.33	0.14	2.28	1.78	1.51	0.90
Tm	0.12	0.15	0.20	0.11	0.05	0.09	0.13	0.21	0.08	0.11	0.05	0.02	0.35	0.30	0.23	0.13
Yb	0.75	0.98	1.24	0.73	0.31	0.57	0.79	1.26	0.53	0.62	0.36	0.17	2.34	2.00	1.46	0.90
Lu	0.11	0.15	0.18	0.12	0.05	0.09	0.12	0.19	0.08	0.09	0.06	0.03	0.35	0.32	0.23	0.14

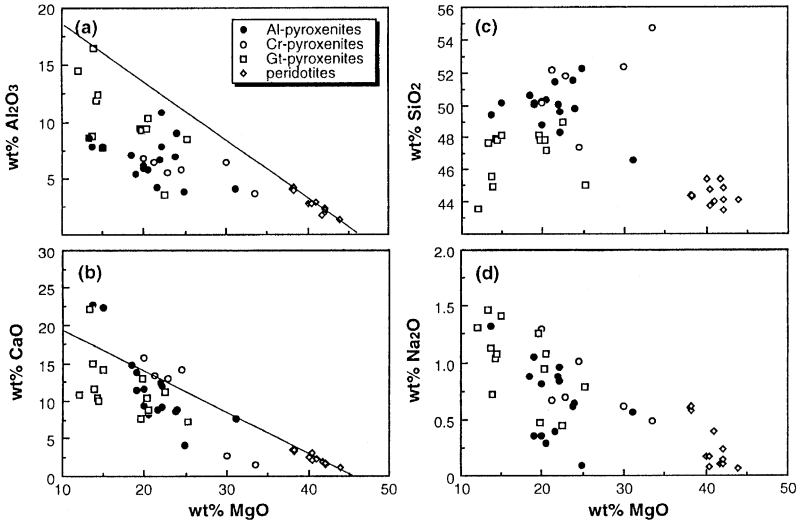

Fig. 2. Variation of selected major oxides (wt.%) versus MgO for pyroxenites from Hannuoba. (a) Al_2O_3 versus MgO; (b) CaO versus MgO; (c) SiO_2 versus MgO; (d) Na_2O versus MgO. Pyroxenite data of Chen et al. (1997) and Zhang et al. (1998a) are included too. The composition of the Hannuoba peridotites (Song and Frey, 1989; Xu, unpublished data) is also shown for comparison. Solid line represents an "extraction" line between the Hannuoba peridotites (as a residue) and calculated equilibrium melt.

variation in both absolute concentration of trace elements and diversity of chondrite-normalized REE pattern (Table 2, Fig. 3).

Most Al-pyroxenites (H-1, H-3, H-4, H-8, H-9) show convex-upward REE pattern which is typical of pyroxene-dominated cumulates (McDonough and Frey, 1989). A very wide range of REE concentration is observed with a total REE of 5.4–84.5 ppm. The apex shifts from Ce to Sm (or Eu) with decreasing REE concentration (Fig. 3a). Sample H-3 is distinct from other Al-pyroxenites by its high REE abundance and the presence of significant negative Eu anomaly. A weak positive Eu anomaly is observed for H-9. In primitive mantle-normalized spider diagram (Fig. 4a), the samples with relatively low REE abundance (H-1, H-8, H-9) show negative anomalies of Zr and Hf and positive U and Rb anomalies. H-1 also displays negative Nb–Ta anomalies, which are not observed for H-8 and H-9. H-3 has pronounced negative Sr and HFSE (high field strength elements: Nb, Ta, Zr, Hf and Ti) anomalies. The clinopyroxenite H-4 has a negative Nb anomaly and very low Rb and Ba contents.

Three Al-pyroxenites (H-2, H-12 and H-13), however, show low LREE/HREE ratios (La/Yb = 0.1–0.7) and REE patterns somewhat similar to those of LREE-depleted lherzolites (Fig. 3b). These samples also show selective enrichment of highly incompatible elements (Fig. 4b). The negative Zr and Hf anomalies are also present but are much less pronounced than those in the Al-pyroxenites with a convex upward pattern.

REE patterns of the Cr-pyroxenites vary depending on their petrographic characteristics. Two Cr-clinopyroxenites (H-5 and H-7) display LREE-enriched pattern with pronounced HFSE depletion compared to the adjacent REE and low Ba contents (Figs. 3c and 4c). This type of pattern differs from the convex-upward ones in much stronger LREE/HREE fractionation. Opx-rich Cr-websterite and orthopyroxenite (H-11, H-14) have considerably low REE concentration consistent with the low abundance of clinopyroxene in these rocks. H-14 has a U-shape REE pattern showing depletion of MREE relative to LREE and HREE (Fig. 3d). H-11 shows a slight LREE-enriched pattern but with HREE/MREE > 1. The particularity of these samples is confirmed in the spider diagram where no HFSE depletion or only weak positive anomalies of HFSE is observed. This may reflect the compensation effect

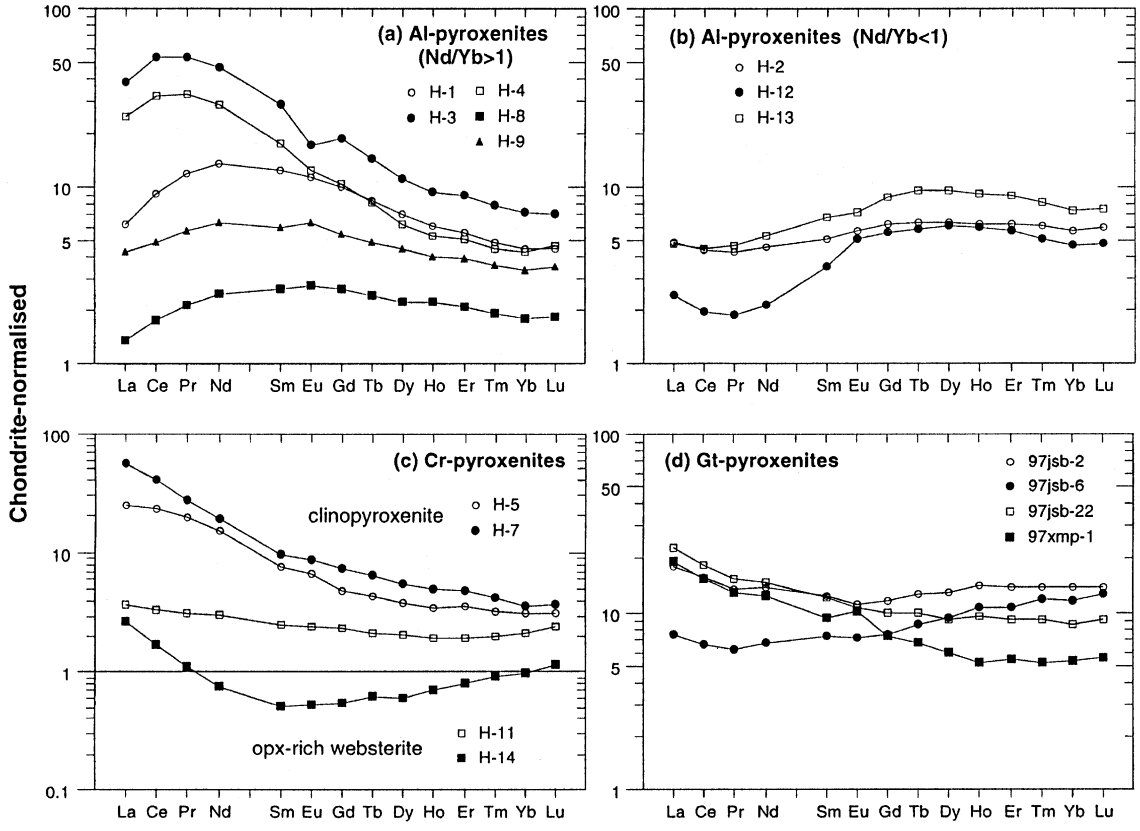

Fig. 3. Chondrite-normalized REE patterns of pyroxenites from Hannuoba. C1 chondrite values from Sun and McDonough (1989). (a) Al-pyroxenites with convex upward pattern; (b) Al-pyroxenites with low La/Yb; (c) Cr-pyroxenites; (d) Garnet pyroxenites.

of orthopyroxene in the bulk rock HFSE budget (Rampone et al., 1991) because of the high Opx/Cpx ratio in the samples.

Both LREE-depleted, LREE-enriched and essentially flat patterns are observed for garnet pyroxenites (Fig. 3d). Sample 97xmp-1 displays an enriched REE pattern with a positive Eu anomaly. The flat pattern of 97jsb-2 is simply a consequence of abundant modal garnet. All garnet pyroxenites are characterized by positive Sr and weak positive Hf anomalies (Fig. 4d).

4.3. Sr–Nd isotopic composition

The analyses in this study were mainly concentrated on whole rocks rather than mineral separates favored by many researchers. However, the Hannuoba xenoliths are generally fresh and a careful selection has been performed to ensure no visible grain-boundary alteration and basaltic veins in the samples. The contribution of grain boundary components to the whole rock compositions is considered to be not important because most samples have very high concentrations of trace elements and some analyses of minerals and bulk rocks from the same samples generally show consistent results (Tatsumoto et al., 1992). The confidence of this inference is encouraged by the fact that the feature presented below such as extremely enriched isotopic compositions and Sr–Nd isotopic decoupling have already been documented (Tatsumoto et al., 1992).

Sr and Nd isotope data of the Hannuoba pyroxenites (Table 3), together with the published data of Chen et al. (1997) and Zhang et al. (1998b) are

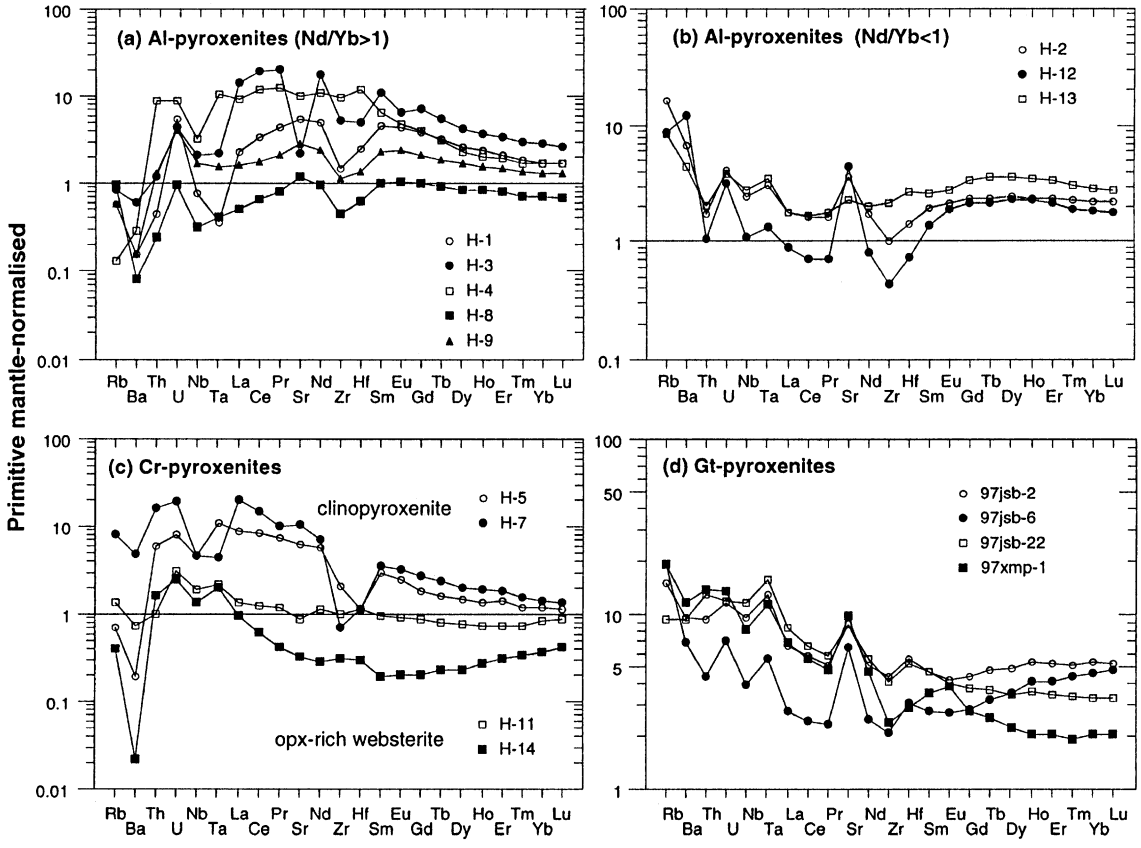

Fig. 4. Primitive mantle normalized element concentration diagram of the pyroxenites from Hannuoba. Normalizing data from Sun and McDonough (1989). Note the strong depletion of HFSE relative to the adjacent REE in some samples.

plotted in Sr–Nd isotopic space (Fig. 5). The data of peridotite xenoliths (Song and Frey, 1989; Tatsumoto et al., 1992; Xu, unpublished data) and isotopic range of basalts (Song et al., 1990; Basu et al., 1991) are also shown for comparison. The Sr and Nd isotope ratios have been corrected for radioactive decay to 135 Ma, which is the approximate age of most pyroxenites (see Section 5.3). The Hannuoba pyroxenites exhibit an extremely wide variation in Sr and Nd isotope composition (Fig. 5) ranging from typical depleted mantle (DM) to crust-like enriched end member (close to EMII). This contrasts with the data of peridotites and Cenozoic basalts that mostly cluster within the depleted mantle domain ($\varepsilon_{Nd} > 0$, $^{87}Sr/^{86}Sr < 0.7045$). Among the pyroxenites from worldwide occurrences, only some pyroxenite xenoliths from SE Australia (Griffin et al., 1988), orogenic pyroxenites of Beni Bousera (Pearson et al., 1993), Bohemian Massif (Medaris et al., 1995) and Lower Austria (Becker, 1996) show similar wide composition range and enriched mantle components (Fig. 6).

Although the Al-pyroxenites have a wide variation in isotope composition with ε_{Nd} of -25 to $+9$ and $^{87}Sr/^{86}Sr$ of 0.7025–0.7113, the majority of them is confined to the field of enriched mantle (Table 2; Fig. 5). Similar extremely enriched mantle composition was documented by Tatsumoto et al. (1992) for a phlogopite pyroxenite from the same locality. The Sr–Nd isotopic data of most Al-pyroxenites are negatively correlated and fall along a trend different from that of MORB–OIB–IAB–sediment (Fig. 5). H-12 has $\varepsilon_{Nd} > 34$ which may be the most radiogenic among the published Nd isotopic data for

Table 3
Whole rock Rb–Sr and Sm–Nd isotopic and concentration data for the Hannuoba pyroxenites

Sample no.	Rb (ppm)	Sr (ppm)	$^{87}Rb/^{86}Sr$ (0 Ma)	$^{87}Sr/^{86}Sr$ (0 Ma)	$^{87}Sr/^{86}Sr$ (135 Ma)	Sm (ppm)	Nd (ppm)	$^{147}Sm/^{144}Nd$ (0 Ma)	$^{143}Nd/^{144}Nd$ (0 Ma)	ε_{Nd} (0 Ma)	ε_{Nd} (135 Ma)
Al-pyroxenites											
H-1	0.913	86.27	0.03064	0.707806 ± 16	0.707747	1.674	5.607	0.1806	0.511778 ± 5	−16.8	−16.5
H-3	0.433	33.52	0.03737	0.710714 ± 13	0.710642	3.943	39.580	0.0603	0.511235 ± 10	−27.4	−25.0
H-4	0.134	160.5	0.00241	0.711305 ± 18	0.711300	2.362	12.000	0.1191	0.511392 ± 8	−24.3	−23.0
H-8	0.524	18.17	0.08358	0.705618 ± 10	0.705458	0.349	1.016	0.2080	0.512609 ± 6	−0.6	−0.8
H-9	1.580	45.40	0.1008	0.705997 ± 14	0.705804	0.825	2.631	0.1896	0.512300 ± 9	−6.6	−6.5
H-12	4.822	70.23	0.1988	0.708734 ± 20	0.708353	0.487	0.923	0.3189	0.514390 ± 7	34.2	32.1
H-12 (duplicate)	5.179	69.35	0.2162	0.708700 ± 20	0.708319	0.473	0.927	0.3088	0.514601 ± 7	38.3	36.4
H-13	5.463	39.42	0.4013	0.705637 ± 12	0.704867	0.895	2.280	0.2376	0.512981 ± 6	6.7	6.0
Cr-pyroxenites											
H-5	0.550	99.77	0.01595	0.703823 ± 18	0.703792						
H-11	3.991	13.43	0.8604	0.704321 ± 14	0.702670	0.427	1.290	0.2001	0.512720 ± 8	1.6	1.5
H-14	0.244	5.30	0.1333	0.704371 ± 15	0.704115	0.075	0.332	0.1369	0.512733 ± 19	1.9	2.9
Garnet pyroxenites											
97jsb-2	8.872	157.8	0.1628	0.706548 ± 15	0.706236	1.563	5.104	0.1852	0.512996 ± 8	7.0	7.2
97jsb-6	11.010	120.6	0.2644	0.706580 ± 14	0.706073	0.853	2.388	0.2160	0.513032 ± 8	7.7	7.4
97jsb-22	5.491	157.7	0.1008	0.706167 ± 19	0.705974	1.631	5.860	0.1684	0.512892 ± 10	5.0	5.4
97xmp-1	12.770	163.0	0.2270	0.706104 ± 14	0.705668	1.132	4.418	0.1550	0.512543 ± 6	−1.9	−1.1

the mantle xenoliths from eastern China. Replicate analyses on this sample yield virtually identical Sr isotopic ratio, variable but consistently high ε_{Nd} (Table 3).

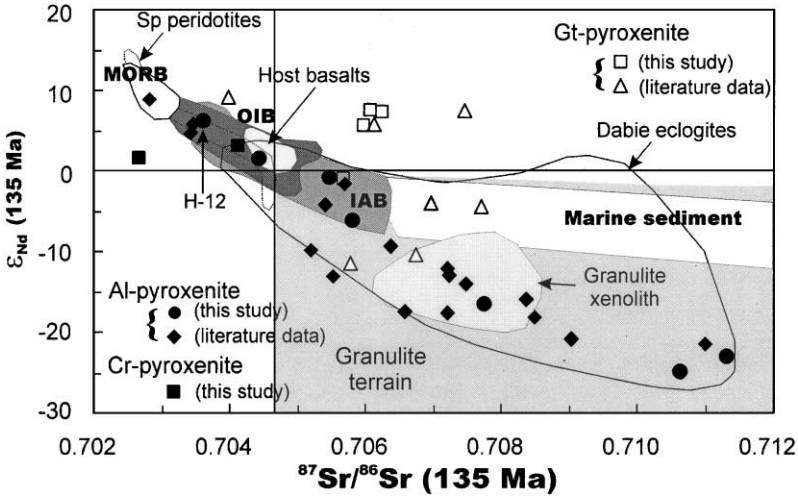

Fig. 5. ε_{Nd} versus $^{87}Sr/^{86}Sr$ (calculated at 135 Ma) of pyroxenites from the Hannuoba pyroxenites. The isotopic composition of H-12 is calculated back to 1.8 Ga. Also shown are the published data of Chen et al. (1997) and Zhang et al. (1998b). Isotope data of the spinel peridotites, granulite xenoliths and Miocene basalts are after Song and Frey (1989), Tatsumoto et al. (1992), Song et al. (1990) and Xu (unpublished data). The fields of eclogites from Dabie ultrahigh pressure metamorphic terran and granulite terrain are from Li et al. (1993) and Chavagnac and Jahn (1996). Marine sediment data are after Ben Othman et al. (1989) and McLennan et al. (1990). MORB and OIB domains are from Zindler and Hart (1986). The fields of different reservoirs are estimated at 135 Ma.

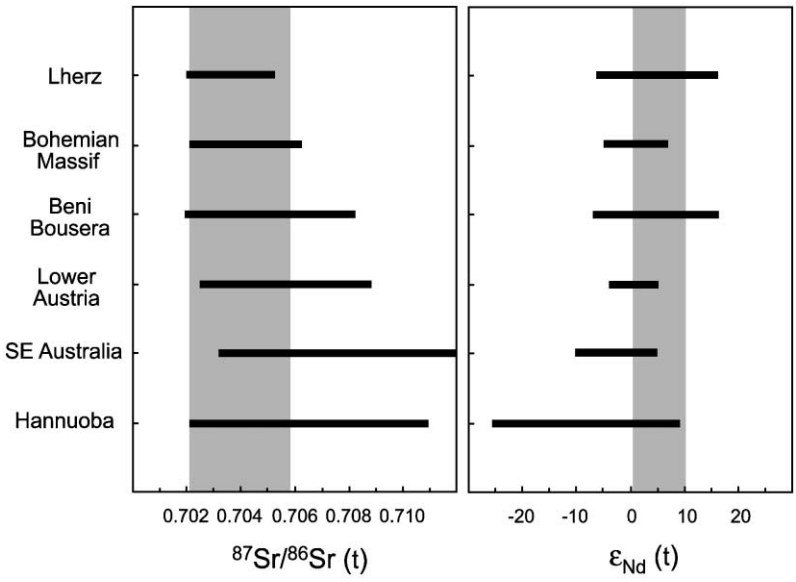

Fig. 6. Comparison of initial Sr and Nd siotopic composition between the Hannuoba pyroxenites and selected orogenic pyroxenite layers and pyroxenite xenoliths. Data are after Becker (1996), Griffin et al. (1988), Medaris et al. (1995) and Pearson et al. (1993). The shaded area stands for the compositional range for the majority of pyroxenites from worldwide occurrence.

In a ε_{Nd} versus Sm/Nd plot (Fig. 7a), the Al-pyroxenites form a broadly positive correlation. If this positive correlation is an isochron, the slope corresponds to an age of 1.9 Ga. Alternatively, this positive correlation may represent a two-component mixing line. Lack of correlation between Rb/Sr and Sr may be related to the disruption of Rb/Sr due to the mobility of both elements during post-formation processes.

The Cr-pyroxenites have a relatively limited range of ε_{Nd} and $^{87}Sr/^{86}Sr$ despite a significant range of Rb/Sr (Table 3). Two opx-rich pyroxenites (H-11, H-14) have indistinguishable isotopic composition (Table 3).

The garnet pyroxenites do not show a simple correlation in the Sr–Nd isotopic diagram despite their relatively wide variation range. They have relatively high $^{87}Sr/^{86}Sr$ ratios at given ε_{Nd} relative to the general trend defined by other two groups of samples (Fig. 5). Three out of four garnet pyroxenites analysed in this study have ε_{Nd} within the range of MORB. The garnet pyroxenites show large scatter in a ε_{Nd}–Sm/Nd plot without any correlation (Fig. 7a).

5. Discussion

5.1. High-pressure cumulates and the nature of parental melts

An important question in the petrogenetic study of pyroxenites is whether they represent frozen melts (e.g., Bodinier et al., 1987; Suen and Frey, 1987; Pearson et al., 1993). This hypothesis can be evaluated by comparing the pyroxenites with melts generated by peridotite melting experiments at high pressures (e.g., Hirose and Kushiro, 1993). In general, the Hannuoba pyroxenites are compositionally different from the melts generated by melting peridotite KLB-1 (e.g., Hirose and Kushiro, 1993), whose composition is similar to the fertile peridotites from Hannuoba (Song and Frey, 1989). Specifically, the pyroxenites have higher MgO contents, either lower or higher SiO_2 and CaO contents than experimental melts. The extremely variable Ni contents (25–1773 ppm) are out of the compositional range predicted by theoretical modeling for the products of partial melting. When plotted against a fractionation index such as MgO (Fig. 2), major element data do not plot

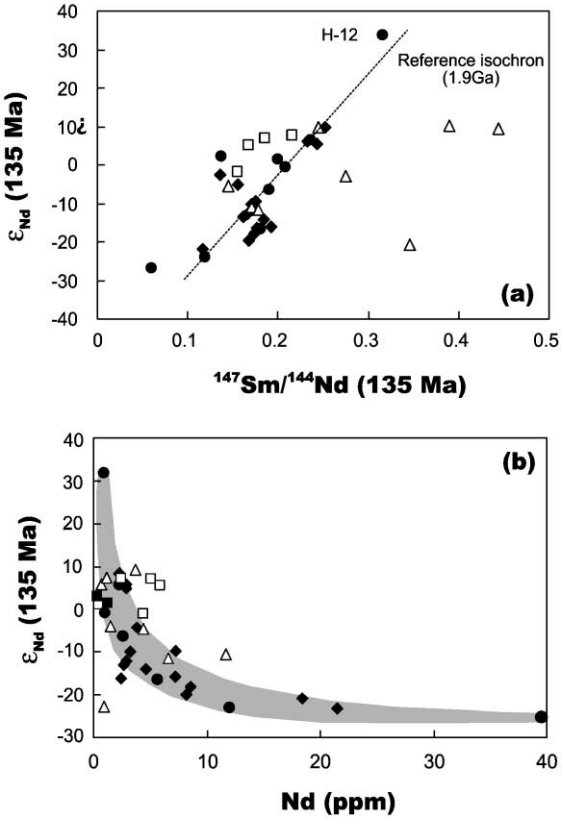

Fig. 7. (a) Sm–Nd isochron diagram and (b) correlation between $^{143}Nd/^{144}Nd$ and Nd for pyroxenites from Hannuoba.

along the "extraction" line between residual and fertile peridotites (Suen and Frey, 1987; Pearson et al., 1993) but show considerable scatter. Therefore, the Hannuoba pyroxenites are neither crystallized melts nor melts extracted from the peridotites.

Other popular ideas on the petrogenesis of pyroxenites vary between two extremes: solid-state recycling oceanic lithosphere (Allegre and Turcotte, 1986) and magmatic segregates precipitated in vein conduits (Irving, 1980). The extreme isotopic variation such as observed in the Hannuoba pyroxenites has led some authors (e.g., Allegre and Turcotte, 1986) to suggest that they represent fragments of recycled oceanic lithosphere of varying ages, thinned by diffusion and convection. However, this model is not suitable for the Hannuoba case where abundant Al-pyroxenite/peridotite and Cr-pyroxenite/peridotite composites and rare composites of garnet clinopyroxenite-lherzolite are found. This and the preserved cumulate texture (modal layering) in some pyroxenites are consistent with a magmatic origin rather than a solid-state recycling of subducted lithosphere. The strong correlation between elemental geochemistry and modal mineralogy, high Al_2O_3 and positive correlation between Mg# and compatible elements such as Ni and Sc are consistent with fractional crystallization model. It is thus concluded that the Hannuoba pyroxenites represent fractionally segregated products from melts at high pressures.

While the very low abundances of incompatible elements in most Al-pyroxenites are consistent with this argument, other samples, particularly garnet pyroxenites, show relatively high contents of Rb, Ba and Th, indicating the presence of small amount of trapped melts. For this reason, composition of melts parental to pyroxenites can only be estimated from the samples with low highly incompatible elements. For the samples that may have trapped melts, the calculation is limited to REE. The calculation was done by applying mineral partition coefficients and mineral modes. The mineral modes are estimated from bulk major element and mineral chemistry using an inversion method. The partition coefficients used in these calculations are taken from the compilation of Becker (1996) except for U, Th, Rb and Ba, which are from Hart and Dunn (1993) and Hauri et al. (1994).

The parental melts of the Al-pyroxenites are highly variable in LREE abundances with $(La/Yb)_N$ ranging from 30 to 400 (Fig. 8). Some of melts have low REE concentrations and display a flat distribution pattern, similar to the host basalts (Basu et al., 1991; Zhi et al., 1990). However, the majority of estimated melts show very high LREE enrichment (La_N = 180–400) that exceeds the range of the Cenozoic basalts. Some of melts are also characterized by negative HFSE anomalies and in some cases Eu anomalies and high Sr isotope and low Nd isotope ratios. These features contrast sharply with the Hannuoba basalts (Song et al., 1990; Zhi et al., 1990; Basu et al., 1991), implying that there is no direct genetic relationship between the majority of pyroxenites and the Cenozoic volcanism. Mantle-derived magmas with similar trace element and isotopic compositions include, island arc basalts, potassic and ultrapotassic magmas, kimberlites, lamproites and

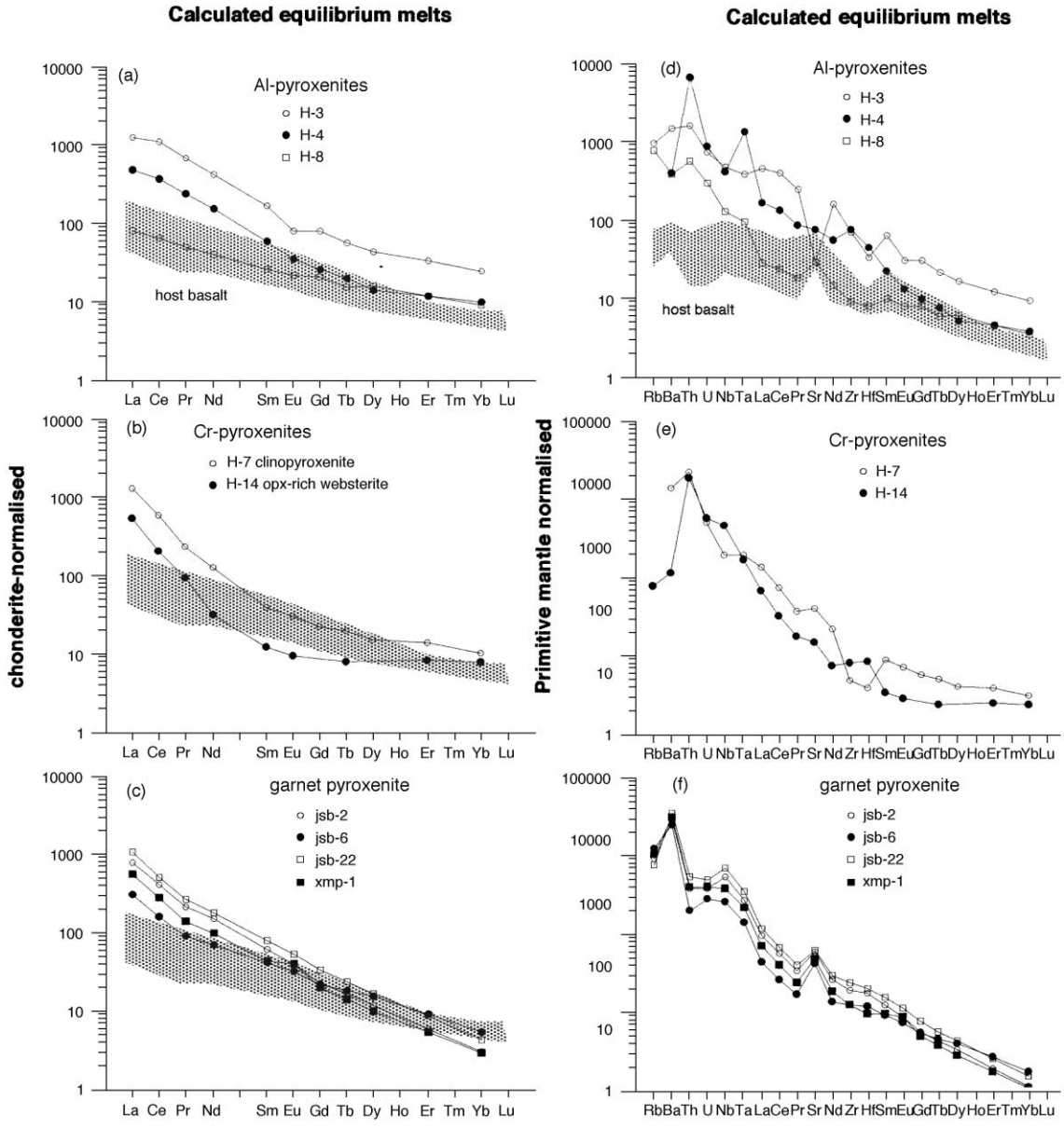

Fig. 8. Normalized REE patterns and spiderdiagrams for melts in equilibrium with pyroxenites from Hannuoba. The patterns are calculated using bulk rock composition and mineral–liquid partition coefficients listed by Becker (1996), Hart and Dunn (1993) and Hauri et al. (1994). The data of host basalts are after Liu et al. (1994) and Zhi et al. (1990).

carbonatites (Becker, 1996). But the assessment of these candidates is not straightforward.

The parental magma in equilibrium with the Cr-pyroxenites has a very steep LREE distribution but an almost flat HREE (Fig. 8b). Such a pattern is different from those of the alkaline basalts. In contrast to the compositional diversity of parental melts for the Al-pyroxenites, the calculated melt compositions for the garnet pyroxenites show relatively coherent trace element distribution patterns (Fig. 8c).

Specifically, the steep REE patterns, low Yb contents, positive Sr anomalies and absence of HFSE anomalies for the melts of garnet pyroxenites are different from those for Al-pyroxenites.

The highly variable REE concentrations of the parental melts of the Hannuoba pyroxenites suggest that they cannot have been formed through crystallization from a single progressively fractionating mafic liquid. In other words, they likely represent crystallization products of different magmatic series. Additional support for this argument is provided by the absence of any correlation between degree of LREE enrichment and Mg#. For instance, some pyroxenites with low Mg# have lower REE concentrations than the samples with high Mg#. The most convincing evidence for non-cogenetic origin of pyroxenites is perhaps from the Sr–Nd isotopic composition which indicates that melts derived from distinct sources were involved in pyroxenite genesis (see Sections 5.4 and 5.5).

5.2. Evidence for metasomatic enrichment in pyroxenites

Melts parental to pyroxenites are frequently considered as important agent of mantle metasomatism (Menzies et al., 1985; Bodinier et al., 1990). However, pyroxenites themselves may be metasomatized too (Garrido and Bodinier, 1999). This is evidenced by an inflection at Ce in the MREE-depleted pattern (Fig. 3b) and selective enrichment of highly incompatible elements over moderately incompatible elements in some Hannuoba pyroxenites (Fig. 4b). Such a distribution pattern is similar to those frequently observed in lherzolite peridotites (McDonough and Frey, 1989; Bedini et al., 1997; Xu et al., 1998) and can be attributed to chromatographic effect of melt percolation (Navon and Stolper, 1987). However, chromatographic effect cannot explain the absolute enrichment of highly incompatible elements in other Hannuoba pyroxenites (Fig. 4d). This requires the combination of chromatographic effects with fractional solidification of melts during their migration down lithospheric thermal gradients (Bedini et al., 1997). The metasomatic agent for the Hannuoba pyroxenites could be either extraneous or the same melt that crystallized the pyroxenites, if the remaining melt fraction is small and if it percolates through the rock while reacting.

5.3. Constraints on the ages of pyroxenites

The extremely high ε_{Nd} in H-12 must reflect time-integrated radiogenic growth in the lithospheric mantle given its high Sm/Nd ratio (Table 3). A single-stage Nd model age of 1.79 Ga relative to the depleted mantle or 2.1 Ga relative to CHUR. This age is comparable with the model age estimated for lherzolites from the same locality (Song and Frey, 1989). The ε_{Nd} of H-12 at 1.8 Ga is $+6$, suggesting a deviation from slightly depleted mantle source. If this model age is accepted as the age of intrusion, a question arises as to whether this age is applicable to other pyroxenites from Hannuoba. The following considerations lead us to propose that the Hannuoba pyroxenites may have formed at different time and most pyroxenites are relatively young.

(a) The positive correlation between ε_{Nd} and Sm/Nd for the Al-pyroxenite (Fig. 7a) yields an apparent isochron age of 1.9 Ga. If this age is meaningful, it implies that all Al-pyroxenites formed simultaneously, and measured isotopic ratios reflect the long-term radiogenic decay in the lithosphere. However, if the isotopic ratios of the Al-pyroxenites are calculated back to this age, the negative Sr–Nd isotopic correlation and positive correlation between ε_{Nd} and Sm/Nd break down. It is very improbable that the pyroxenites, which originally scattered in the Sr–Nd space form a negative correlation after the radioactive decay with time. Moreover, the most radiogenic Sr isotopic compositions are noted in the samples with very low Rb/Sr ratios (H-1, H-3 and H-4). Therefore, not all isotopic composition can be interpreted as a result of in-situ radioactive decay. The positive correlation in Fig. 7a more likely represents a two-component mixing line. This is supported by the hyperbolic correlation between ε_{Nd} and Nd for the Al-pyroxenites (Fig. 7b). The good correlation further suggests that radiogenic growth since mixing has not significantly affected the mixing relationship, given the wide range of Rb/Sr and Sm/Nd. It is likely that mixing is relatively recent and most Al-pyroxenites (except for H-12, probably H-13 as well) have a relatively young intrusion age.

This argument is consistent with the isotopic disequilibrium between Al-pyroxenite vein and host peridotites (Tatsumoto et al., 1992).

(b) A young age can also be inferred for the Cr-pyroxenites because they have very limited variation in $^{87}Sr/^{86}Sr$ despite a wide range of Rb/Sr. This inference is consistent with the igneous appearing texture in these samples, and the isotopic disequilibrium between Cr-pyroxenite vein and host peridotites (Song and Frey, 1989). A similar conclusion is reached for the garnet pyroxenites by Zhang et al. (1998a,b) on the basis of Pb isotopic data.

(c) The marked contrast in isotopes between pyroxenite xenoliths and host basalts suggest they are not cogenetic. The pyroxenites may have formed prior to the eruption of lavas (Miocene). The negative Sr–Nd isotopic correlation breaks down when the correction age is greater than 200 Ma. It is possible that the intrusion age of pyroxenites is less than 200 Ma. For the convenience of presentation, we arbitrarily choose 135 Ma for the age correction of isotopic ratios. This age corresponds to the period of the dramatic lithospheric thinning (Menzies et al., 1993; Griffin et al., 1998) and basaltic underplating (Fan et al., 1998) beneath the Sino-Korean Craton. Such a late Mesozoic age is also confirmed by the recent dating on zircons from the Hannuoba Al-pyroxenites and garnet pyroxenites using SHRIMP at Curtin University, Australia (X.H. Zhou, personal communication). Preliminary results show a rather wide age spectrum ranging from 4.3 Ga to 80 Ma but with peaks at the late Mesozoic.

5.4. Garnet-pyroxenites: an altered oceanic crust model

If the melts parental to the pyroxenites were subduction-related, the pyroxenites should plot in or above the MORB–OIB–IAB–sediment trend. As shown in Fig. 5, some garnet pyroxenites show relatively high $^{87}Sr/^{86}Sr$ at given ε_{Nd} compared to the mantle array and the MORB–OIB–IAB–sediment trend (Fig. 5). Such a Sr–Nd isotopic decoupling is consistent with their respective elemental concentrations. While Sr occurs as a spike in spider diagram, Nd and other moderately incompatible elements form a smooth depletion trend. This suggests that a component rich in Sr but containing little Nd may have been involved in the source of garnet pyroxenites. Similar Sr–Nd isotopic decoupling and trace element characteristics are observed for pyroxenites from Beni-Bousera (Pearson et al., 1993) and the Bohemian Massif (Medaris et al., 1995) which has been attributed to the involvement of subducted oceanic lithosphere in the pyroxenite source. A similar model is thus envisaged for the garnet pyroxenites from Hannuoba. It has been demonstrated that altered oceanic basalt displays a relatively constant ε_{Nd} and a wide $^{87}Sr/^{86}Sr$ ratio (McCulloch et al., 1980) because sea water is extremely low in Nd concentration (O'Nions et al., 1978). The low ε_{Nd} values in some samples further suggest that sedimentary components may have been involved in the source. Fig. 9 shows a pattern of mixture between seawater altered oceanic crust and trench sediment. Such a mixture would define a roughly triangular area that can enclose the irregular distribution of Sr–Nd isotope data of most garnet pyroxenites.

In this sense, there is a two-stage process by which the observed Sr–Nd isotope composition of garnet pyroxenites formed. First, seafloor hydrothermal alteration of oceanic basalts resulted in a wide variation in $^{87}Sr/^{86}Sr$ but left their ε_{Nd} nearly unaffected. Second, mixing of altered basalts and cover sediment may have occurred during subduction. The addition of sediment lowered ε_{Nd} in the system. The melting of such a mixture was probably triggered by the presence of fluid dehydrated from the subducting slab. This mechanism requires that the part of the lithosphere beneath Hannuoba may represent a paleo-convergent plate margin, and is consistent with the geological history of the region. Hannuoba is located to the northern boundary of the Sino-Korean Craton. Along this boundary, the late Jurassic E–W-trending fold-and-thrust belt can be traced from Liaoning province (east) to the eastern Tian Shan (west) (Yin and Nie, 1996). This contractional deformation was both spatially and temporally associated with emplacement of plutons and was followed by early Cretaceous extension. The fold-and-thrust belt may have been generated by southward subduction of the Mongol–Okhotsk plate beneath the Sino-Korean Craton and/or collision between the Sino-Korean Craton and the Yangtze Craton (Yin and Nie, 1996). Most of the garnet pyroxenites could have formed at such a convergent setting.

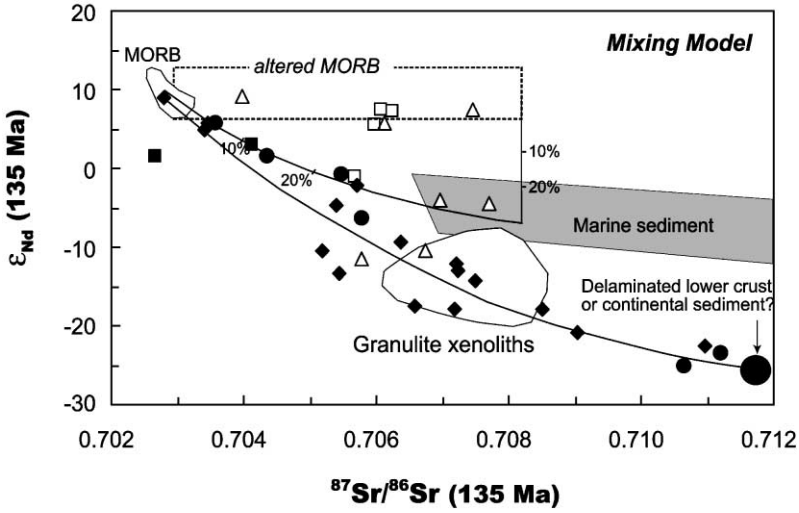

Fig. 9. Diagram showing mixing models for the genesis of the Hannuoba pyroxenites. Note that the most variability of the Al-pyroxenites and Cr-pyroxenites can be accounted for by a mixing between an asthenospheric mantle and a crustal component from the Sino-Korean Craton (terrigenous sediment or delaminated lower crust). An altered oceanic crust, however, may be involved in the source for the garnet pyroxenites. The field of altered MORB is after McCulloch et al. (1980). Tick marks show the effect of sediment addition.

The Sr–Nd isotopic data of two garnet pyroxenites are plotted out of the triangular mixing area and instead plotted along the distribution trend defined by the Al-pyroxenites (Fig. 9). A continental crustal component is required in the source of these pyroxenites. The involvement of continental crustal components is more evident in the petrogenesis of the Al-pyroxenites.

5.5. Al- and Cr-pyroxenites: involvement of continental crustal components in the source

A few Al- and Cr-pyroxenites show Sr–Nd isotopic compositions similar to MORB and host basalts and they may have been derived from an asthenospheric melt. However, the majority of the pyroxenites display higher $^{87}Sr/^{86}Sr$ and lower ε_{Nd} relative to the host basalts (Fig. 5). This suggests that the parental magmas of most Hannuoba pyroxenites were derived from a source significantly different from the asthenosphere from which alkali basalts were generated (Song et al., 1990). Negative Zr and Hf anomalies in some Al- and Cr-pyroxenites from Hannuoba (Fig. 4) could be related to tiny zircons, which were not dissolved in Savillex breakers. However, only a limited number of pyroxenite samples contain zircon (X.H. Zhou, personal communication). Moreover, HFSE depletion is also present in the samples which contain no zircon (Zhang et al., 1998a; X.H. Zhou, personal communication). Thus, HFSE anomalies in the Hannuoba pyroxenites are real and not analytical artifacts. It is interesting to note that HFSE anomalies are lacking in the peridotite xenoliths from Hannuoba (Xu et al., unpublished data) and in modally metasomatized peridotites in general (McKenzie, 1989). Therefore, peridotites cannot be the only source of parental magmas of the Al-pyroxenites.

As discussed previously, the isotopic composition of the Al-pyroxenites can be accounted for by mixing of a depleted mantle component and a crust-like component. Most Al-pyroxenites plot below the MORB–OIB–IAB–sediment trend falling in the granulite area (Fig. 5). This suggests that the enriched component may have had a long residence time in the crust with relative lower Sm/Nd and Rb/Sr ratios. However, both pyroxenite-peridotite composite and geothermometric calculations suggest that most of pyroxenites originated in the mantle. This requires the recycling of crustal materials to the mantle. In the following, possible origin of this continental component and its implication for the crustal recycling mechanism will be discussed.

Isotopic studies show that sedimentary rocks from the Sino-Korean Craton are old with T_{DM} varying between 2.5–3.6 Ga (Wu, 1998). Their $^{143}Nd/^{144}Nd$ ratio at 135 Ma varies between 0.5110 and 0.5115. The mixing between the asthenosphere and terrigenous sediments from the Sino-Korean Craton could account for the entire range of isotopic compositions of the Al-pyroxenites. In this sense, the isotopic data of the Al-pyroxenites are consistent with a subduction or a collision model presented for the garnet pyroxenites. The implication of this model is that the Al-pyroxenites and garnet pyroxenites formed contemporaneously at a convergent setting.

Alternatively, the enriched component may represent the lower crust of the Sino-Korean Craton. Hannuoba is situated within an Archean crust whose basement experienced a long-term evolution. It is thus possible that the Hannuoba pyroxenites represent products of a contaminated asthenospheric melt when it underplated at the crust–mantle boundary. However, the granulite xenoliths in the Miocene basalts that formed essentially in this way show a rather limit range in Sr–Nd isotopic composition (Fig. 9; Fan et al., 1998; Zhang et al., 1998b). This contrasts with the extremely wide isotopic range of the Hannuoba pyroxenites. In other words, the current lower crust beneath Hannuoba does not have sufficient Sr–Nd isotopic variation to account for the entire isotopic variation in the pyroxenites (Fig. 5). Moreover, such a mechanism is at variance with the location of these pyroxenites within the upper mantle as revealed by numerous peridotite-pyroxenite composites. U–Pb zircon dating suggests that these granulite xenoliths are relatively young (about 135 Ma; Fan et al., 1998). It is likely that the present lower crust is significantly different from the previously existed one which may be compositionally represented by the exhumed granulite terrain (e.g., TTG) and was delaminated during the late rejuvenation of lithospheric mantle.

Considerably different thermal gradient and composition have been inferred for the Palaeozoic and Cenozoic lithosphere beneath the Sino-Korean Craton (Griffin et al., 1998; Menzies and Xu, 1998). This has led to the suggestion that the Palaeozoic, cold and thick lithospheric keel (>150 km) has been gradually eroded as a result of passive upwelling of the lower convective asthenosphere since the late Mesozoic. Delamination has also been proposed as an important mechanism to account for the intermediate composition of the continental crust (Arndt and Goldstein, 1989; Rudnick and Fountain, 1995). This model has recently been adopted by Gao et al. (1998) to account for the crustal evolution in the Sino-Korean Craton. Based on a regional geochemical study of fine-grained clastic sediment, these authors concluded that the delaminated crust is compositionally similar to the exhumed eclogites in Dabie ultrahigh pressure metamorphic zone.

The enriched components in the Al-pyroxenites fall within the granulite terrain area (Fig. 5). It is also noted that the Dabieshan eclogites encompass enriched components of the Hannuoba pyroxenites (Chavagnac and Jahn, 1996), and in particular the Type II eclogites display a Sr–Nd isotopic trend very similar to that defined by the Al-pyroxenites from Hannuoba (Li et al., 1993). It is thus likely that the Al- and Cr-pyroxenites resulted from interaction between asthenosphere-derived melts and delaminated lower crust. The formation of the Al-pyroxenites may comprise two stages: (1) foundering of the eclogite root to the peridotite mantle took place probably during lithospheric thinning that started since the Mesozoic (Griffin et al., 1998; Menzies and Xu, 1998); (2) as a response of initial lithospheric thinning, asthenosphere containing blobs of delaminated lower crust melted adiabatically. Fractionation of melting products within the lithospheric mantle gave rise to the formation of the Al-pyroxenites.

The above alternatives (i.e., subduction of continental upper crust versus delamination of lower crust) are not mutually exclusive. However, given the close association between mineralogy and isotopic compositions of the pyroxenites, we favor the second alternative. With this interpretation, the Al-pyroxenites may have formed at an extensional setting, probably coeval with the lithospheric thinning beneath the Sino-Korean Craton. If it is the case, the Al-pyroxenites may be young relative to the garnet pyroxenites.

5.6. Implications for mantle enrichment and intraplate magmatic generation

Peridotite xenoliths from eastern China commonly show sign of metasomatism (Song and Frey, 1989; Xu et al., 1998). Compared with unmetasomatised

peridotites, metasomatised xenoliths generally have higher $^{87}Sr/^{86}Sr$ and lower ε_{Nd}, trending toward the bulk earth values. The peridotites adjacent to pyroxenite veins show conspicuously higher Sr and lower Nd isotope ratios compared to the discrete peridotite xenoliths, strongly suggesting the possible role of pyroxenites and its deviates in mantle metasomatism (Song and Frey, 1989). Nevertheless, given the relatively small volume represented by pyroxenites, the corresponding modification of lherzolite would be relatively small and the significant modification is generally confined to the vicinity of the veins. Geochemical studies (Song and Frey, 1989; Tatsumoto et al., 1992) on the spinel peridotites from Hannuoba have revealed that the lithosphere at this area had a very depleted feature since the Archean. This lithosphere has subsequently been modified by the mutiple metasomatism, notably at 1 Ga by fluid associated with continental accretional processes, and more recently by metasomatism associated with subducted slab-derived fluids at <500 Ma (Song and Frey, 1989; Tatsumoto et al., 1992). The data presented in this study imply that metasomatic agent could be either subducted-related fluids or delaminated lower crust derived.

The pyroxenite-veined mantle has been invoked as the source of certain continental magmas (Leeman and Harry, 1993). The pyroxenite solidus is at lower temperature than peridotite solidi (Hirschmann and Stolper, 1996). It is expected that in upwelling mantle comprising mixed pyroxenite and peridotite, the pyroxenites will begin melting deeper than the peridotite (Hirschmann and Stolper, 1996). The depth interval over which pyroxenite is partially melting but peridotites is subsolidus is estimated to be about 15 km by taking account into the solidus slope and adiabatic upwelling path (Hirschmann and Stolper, 1996). This difference thus can sufficiently cause different melting episodes, as exemplified in western USA. It is documented that in North China, the late Cretaceous and early Tertiary basalts and lamporhyres have enriched Sr–Nd isotopic composition ($\varepsilon_{Nd}=-22$ to -5) but are depleted in HFSE, whereas the late Tertiary and Quaternary basalts display isotopic composition typical of depleted mantle and no HFSE anomalies in spiderdiagram (Xu et al., 1995; W.M. Fan, personal communication). The enriched lithospheric mantle has been invoked as source of the early phases of extension-related magmatism, but such a component is not evidenced until recently because most mantle peridotite xenoliths display a depleted isotope signature. The presence of HFSE-depleted and isotopically enriched pyroxenites, as shown in this study, thus provides direct evidence for enriched components in the lithospheric mantle and affirms their participation in early phase of intraplate magmatism. The relatively uniform Sr–Nd isotopic composition of the Hannuoba basalts (Fig. 5) suggests that the source region of these magmas is different from that of pyroxenites.

6. Conclusions

The pyroxenite xenoliths from Hannuoba are heterogeneous in mineralogy, chemistry and isotopic composition. They are neither frozen melts nor solid-state recycled oceanic lithosphere, but are likely high-pressure crystal segregates from parental melts in the lithosphere. Contrary to pyroxenite xenoliths that are usually assumed to de derived from alkali basaltic magmas, the Hannuoba pyroxenites require crustal components in their magmatic source. The Al- and Cr-pyroxenites were generated by mixing an asthenospheric melt with variable amount of continental crust component. This crustal component could be subducted terrigenous sediments from the Sino-Korean Craton or the delaminated long-term evolved lower continental crust. In contrast, a subducted oceanic crust (i.e., hydrothermally altered basalts and sedimentary materials) was involved in the source of melts from which garnet pyroxenites crystallized. Although the age of the Hannuoba pyroxenites is largely unknown, they probably represent products of magmatic events at different time. Except for a few Al-pyroxenites (e.g., H-12) that may be old (~ 2 Ga), most pyroxenites are relatively young, probably of late Mesozoic in age. Taking into account the regional geology and tectonic evolution, we tentatively propose that the garnet pyroxenites were genetically related to the southward subduction of the Mongol–Okhotsk plate beneath North China, whereas the formation of the Al-pyroxenites was coeval with the lithospheric thinning beneath the Sino-Korean Craton during the late Mesozoic. Fur-

ther research is needed to constrain the timing of these petrogenetic processes, which is of critical importance in the verification of the proposed models.

Acknowledgements

The author would like to thank Prof. C.Y. Lin and L.B. Shi for generous donation of garnet-bearing samples, Y. Liu and Z. Qian for their technical help with ICP-MS and major element analyses and Dr. S.-s. Sun for comments on the early version of this paper. Drs. H. Becker, J.-L. Bodinier and R. Rudnick are thanked for their thoughtful and constructive reviews which substantially improved the paper. The financial supports from National Sciences Foundation of China (49925308, 49703042, 49733110) and the Ministry of Sciences and Technology (Grant No: 95-pre-39 project) are gratefully acknowledged.

References

Allegre, C., Turcotte, D.L., 1986. Implications of a two component marble-cake mantle. Nature 323, 123–126.

Arndt, N.T., Goldstein, S.L., 1989. An open boundary between lower continental crust and mantle: its role in crust formation and crustal recycling. Tectonophysics 161, 201–212.

Basu, A.R., Wang, J.W., Huang, W.K., Xie, G.H., Tatsumoto, M., 1991. Major element, REE and Pb, Nd and Sr isotopic geochemistry of Cenozoic volcanic rocks of eastern China: implications for origin from suboceanic-type mantle reservoirs. Earth Planet. Sci. Lett. 105, 149–169.

Becker, H., 1996. Crustal trace element and isotopic signatures in garnet pyroxenites from garnet peridotite massifs from Lower Austria. J. Petrol. 37, 785–810.

Bedini, R.M., Bodinier, J.-L., Dautria, J.M., Morten, L., 1997. Evolution of LILE-enriched small melt fractions in the lithospheric mantle: a case study from the Eastern African Rift. Earth Planet. Sci. Lett. 153, 67–83.

Ben Othman, D., White, W.M., Patchett, J., 1989. The geochemistry of marine sediments, island arc magma genesis and crust–mantle recycling. Earth Planet. Sci. Lett. 94, 1–21.

Bertand, P., Mercier, J.-C., 1986. The mutual solubility of co-existing ortho- and clinopyroxene: towards an absolute geothermobarometer for the natural system? Earth Planet. Sci. Lett. 77, 109–122.

Bodinier, J.-L., Guiraud, M., Fabries, J., Dostal, J., Dupuy, C., 1987. Petrogenesis of layered pyroxenites from the Lherz, Freychinede and Prades ultramafic bodies (Ariege, French Pyrenees). Geochim. Cosmochim. Acta 51, 279–290.

Bodinier, J.L., Vasseur, G., Vernieres, J., Dupuy, C., Fabries, J., 1990. Mechanisms of mantle metasomatism: geochemical evidence from the Lherz orogenic peridotite. J. Petrol. 31, 597–628.

Chavagnac, V., Jahn, B.M., 1996. Coesite-bearing eclogites from the Bixiling Complex, Dabie Mountains, China: Sm–Nd ages, geochemical characteristics and tectonic implications. Chem. Geol. 133, 29–52.

Chen, G.Y., Song, Z.H., An, C.Q., Cheng, L.H., Zhuang, Z., Fu, Z.W., Lu, Z.L., Hu, J.F., 1991. Three dimensional crust and upper mantle structure of the North China region. Acta Geophys. Sin. 34, 172–181 (in Chinese).

Chen, D.G., Zhi, X.C., Li, B.X., Wang, Y.X., Yang, J.D., 1997. Nd, Sr, Pb isotopic compositions and their petrogenetic information of pyroxenite xenoliths from Hannuoba basalts China. Geochimica 26, 1–12 (in Chinese).

Fan, Q.C., Liu, R.X., Li, H.M., Li, N., Sui, J.L., Lin, Z.R., 1998. Zircon geochronology and REE geochemistry of granulite xenoliths from Hannuoba. Chin. Sci. Bull. 43, 133–137 (in Chinese).

Fan, Q.C., Sui, J.L., Liu, R.X., Zhou, X.M., 2001. Eclogite facies garnet-pyroxenite xenolith in Hannuoba area: new evidence of magma underplating. Acta Petrol. Sin. 17, 1–6 (in Chinese with English abstract).

Gao, S., Zhang, B.R., Jin, Z.M., Kern, H., Luo, T.C., Zhao, Z.D., 1998. How mafic is the lower continental crust. Earth Planet. Sci. Lett. 161, 101–117.

Garrido, C.J., Bodinier, J.L., 1999. Diversity of mafic rocks in the Ronda peridotite: evidence for pervasive melt-rock reaction during heating of subcontinental lithosphere by upwelling asthenosphere. J. Petrol. 40, 729–754.

Govindaraju, K., 1989. Compilation of working values and sample description data for 272 geostandards. Geostand. Newsl. 13, 1–114.

Griffin, W.L., O'Reilly, S.Y., Stable, A., 1988. Mantle metasomatism beneath western Victoria, Australia: II. Isotopic geochemistry of Cr-diopside lherzolites and Al-augite pyroxenites. Geochim. Cosmochim. Acta 52, 449–459.

Griffin, W.L., Zhang, A.D., O'Reilly, S.Y., Ryan, G., 1998. Phanerozoic evolution of the lithosphere beneath the Sino-Korean Craton. In: Flower, M., Chung, S.L., Lo, C.H., Lee, T.Y. (Eds.), Mantle Dynamics and Plate Interactions in East Asia. Am. Geophys. Union Geodyn. Ser., vol. 27, pp. 107–126.

Hart, S.R., Dunn, T., 1993. Experimental cpx/melt partitioning of 24 trace elements. Contrib. Mineral. Petrol. 113, 1–8.

Hauri, E.H., Wagner, T.P., Grove, T.L., 1994. Experimental and natural partitioning of Th, U, Pb and other elements between garnet, clinopyroxene and basaltic melts. Chem. Geol. 117, 149–166.

Hirose, K., Kushiro, I., 1993. Partial melting of dry peridotites at high pressures: determination of composition of melts segregated from peridotite using aggregates of diamond. Earth Planet. Sci. Lett. 114, 477–489.

Hirschmann, M.M., Stolper, E.M., 1996. A possible role for

garnet pyroxenite in the origin of the "garnet signature" in MORB. Contrib. Mineral. Petrol. 124, 185–208.

Irving, A.J., 1980. Petrology and geochemistry of composite ultramafic xenoliths in alkali basalts and implications for magmatic processes within the mantle. Am. J. Sci. 280-A, 389–426.

Jahn, B.M., Bernard-Griffiths, J., Charlot, R., Vidal, P., 1980. Nd and Sr isotopic compositions and REE abundances of Cretaceous MORB (Holes 417D and 418A, Legs 51, 52 and 53). Earth Planet. Sci. Lett. 48, 171–184.

Jahn, B.M., Auvray, B., Cornichet, J., Bai, Y.L., Shen, Q.H., Liu, D.Y., 1987. 3.5 Ga old amphibolites from eastern Hebei province China: field occurrence, petrography, Sm–Nd isochron age and REE geochemistry. Precambrian Res. 34, 311–346.

Leeman, W.P., Harry, D.L., 1993. A binary source model for extension related magmatism in the Great Basin, Western North America. Science 262, 1550–1554.

Li, S.G., Xiao, Y.L., Liou, D.L., Chen, Y.Z., Ge, N.J., Zhang, Z.Q., Sun, S.-S., Cong, B.L., Zhang, R.Y., Hart, S.R., Wang, S.S., 1993. Collision of the North China and Yangtze Blocks and formation of coesite-bearing eclogites: timing and processes. Chem. Geol. 109, 89–111.

Liu, C.Q., Masuda, A., Xie, G.H., 1994. Major- and trace-element compositions of Cenozoic basalts in eastern China: petrogenesis and mantle source. Chem. Geol. 114, 19–42.

Liu, Y., Liu, H.C., Li, X.H., 1996. Precise and rapid analyses of 40 trace elements by ICP-MS. Geochimica 25, 410–418 (in Chinese).

Loubet, M., Allegre, C.J., 1980. Trace elements in orogenic lherzolites reveal complex history of the upper mantle. Nature 298, 809–811.

Ma, X., 1989. Lithospheric dynamic altas of China. China Cartographic Publishing House, Beijing, 125 pp.

McCulloch, M.T., Gregory, R.T., Wasserburg, G.J., Taylor, H.P., 1980. A neodymium, strontium, and oxygen isotopic study of the Cretaceous Samail ophiolite and implications for the petrogenesis and sea-water-hydrothermal alteration of the oceanic crust. Earth Planet. Sci. Lett. 46, 201–211.

McDonough, W.F., Frey, F.A., 1989. Rare earth elements in upper mantle rocks. In: Lipin, B., McKay, G. (Eds.), Geochemistry and Mineralogy of Rare Earth Elements. Rev. Mineral., vol. 21, pp. 99–145.

McKenzie, D.P., 1989. Some remarks on the movement of small melt fractions in the mantle. Earth Planet. Sci. Lett. 95, 53–72.

McLennan, S.M., Taylor, S.R., McCulloch, M.T., Maynard, J.B., 1990. Geochemical and Nd–Sr isotopic composition of deep-sea turbidites. Geochim. Cosmochim. Acta 54, 2015–2050.

Medaris, L.G., Beard, B.L., Johnson, C.M., Valley, J.W., Spicuzza, M.J., Jelinek, E., Misar, Z., 1995. Garnet pyroxenite and eclogite in the Bohemian Massif: geochemical evidence for Variscan recycling of subducted lithosphere. Geol. Rundsch. 84, 489–505.

Menzies, M.A., Xu, Y.G., 1998. Geodynamics of the North China Craton. In: Flower, M., Chung, S.L., Lo, C.H., Lee, T.Y. (Eds.), Mantle Dynamics and Plate Interactions in East Asia. Am. Geophys. Union, Geodyn. Ser., vol. 27, pp. 155–165.

Menzies, M.A., Kempton, P.D., Dungan, M., 1985. Interaction of continental lithosphere and asthenospheric melts below the Geronimo Volcanic Field, Arizona, USA. J. Petrol. 26, 663–693.

Menzies, M.A., Fan, W.M., Zhang, M., 1993. Palaeozoic and Cenozoic lithoprobes and the loss of >120 km of Archaean lithosphere, Sino-Korean craton, China. In: Prichard, H.M., Alabaster, T., Harris, N.B.W., Neary, C.R. (Eds.), Magmatic Processes and Plate Tectonics. Geol. Soc. Spec. Publ., vol. 76, pp. 71–78.

Navon, O., Stolper, E., 1987. Geochemical consequence of melt percolation: the upper mantle as a chromatographic column. J. Geol. 95, 285–307.

Nickel, H.G., Green, D.H., 1985. Empirical geothermobarometry for garnet peridotites and implications for the nature of the lithosphere, kimberlites and diamonds. Earth Planet. Sci. Lett. 73, 158–170.

O'Nions, R.K., Carter, S.R., Cohen, R.S., Evensen, N.M., Hamilton, P.J., 1978. Pb, Nd and Sr isotopes in oceanic ferromanganese deposits and ocean flood basalts. Nature 273, 435–438.

Pearson, D.G., Davies, G.R., Nixon, P.H., 1993. Geochemical constraints on the petrogenesis of diamond facies pyroxenites from the Beni Bousera peridotite massif, North Morocco. J. Petrol. 34, 125–172.

Qi, Q., Taylor, L.A., Zhou, X.M., 1995. Petrology and geochemistry of mantle peridotite xenoliths from SE China. J. Petrol. 36, 55–75.

Rampone, E., Botazzi, P., Ottolini, L., 1991. Complementary Ti and Zr anomalies in orthopyroxene and clinopyroxene from mantle peridotites. Nature 354, 518–520.

Remaidi, R., 1993. Etude geochimique de l'association harzburgite-dunite et pyroxenite de l'Arroyo de la Cala (Massif de Ronda, Espagne), PhD Thesis, Univ. Montpellier.

Rudnick, R.L., Fountain, D.M., 1995. Nature and composition of the continental crust: a lower crust perspective. Rev. Geophys. 33, 267–309.

Song, Y., Frey, F.A., 1989. Geochemistry of peridotite xenoliths in basalt from Hannuoba, eastern China: implications for subcontinental mantle heterogeneity. Geochim. Cosmochim. Acta 53, 97–113.

Song, Y., Frey, F.A., Zhi, X.C., 1990. Isotopic characteristics of Hannuoba basalts, eastern China: implications for their petrogenesis and the composition of subcontinental mantle. Chem. Geol. 85, 35–52.

Suen, C.J., Frey, F.A., 1987. Origins of the mafic and ultramafic rocks in the Ronda peridotites. Earth Planet. Sci. Lett. 85, 183–202.

Sun, S.-S., McDonough, W.F., 1989. Chemical and isotopic systematics of oceanic basalts: implications for mantle composition and processes. In: Saunders, A.D., Norry, M.J. (Eds.), Magmatism in the Ocean Basins. Geol. Soc. Spec. Publ., vol. 42, pp. 313–345.

Tatsumoto, M., Basu, A.R., Huang, W.K., Wang, J.W., Xie, G.H., 1992. Sr, Nd, and Pb isotopes of ultramafic xenoliths in volcanic rocks of Eastern China: enriched components EMI and EMII in subcontinental lithosphere. Earth Planet. Sci. Lett. 113, 107–128.

Whilshire, W.M., Shervais, J.W., 1975. Al-augite and Cr-diopside

ultramafic xenoliths in basaltic rocks from the western United States. Phys. Chem. Earth 9, 257–272.

Wu, F.Y., 1998. Age and accretionary process of the continental crust. In: Zheng, Y.F. (Ed.), Chemical Geodynamics. Scientific Press, Beijing, pp. 224–261.

Xu, Y.G., 2001. Thermo-tectonic destruction of the Archaean lithospheric keel beneath eastern China: evidence, timing and mechanism. Phys. Chem. Earth, in press.

Xu, Y.G., Fan, W.M., Lin, G., 1995. Lithosphere-asthenosphere interaction: a comparative study on Cenozoic and Mesozoic basalts around Bohai area. Geotecton. Metallog. 19, 1–13.

Xu, X.S., O'Reilly, S.Y., Zhou, X.M., Griffin, W.L., 1996a. A xenolith-derived geotherm and the crust–mantle boundary at Qilin, southeastern China. Lithos 38, 41–62.

Xu, Y.G., Menzies, M.A., Mattey, D.P., Lowry, D., Harte, B., Hinton, R.W., 1996b. The nature of the lithospheric mantle near the Tancheng-Lujiang fault, China: an integration of texture, chemistry and O isotopes. Chem. Geol. 134, 67–82.

Xu, Y.G., Menzies, M.A., Vroon, P., Mercier, J.C., Lin, C.Y., 1998. Texture–temperature–geochemistry relationships in the upper mantle as revealed from spinel peridotite xenoliths from Wangqing, NE China. J. Petrol. 39, 469–493.

Xu, Y.G., Lin, C.Y., Shi, L.B., 1999. The geotherm of the lithosphere beneath Qilin, SE China: a re-appraisal and implication for P–T estimation of Fe-rich pyroxenites. Lithos 47, 181–193.

Yin, A., Nie, S.Y., 1996. A Phanerozoic palinspastic reconstruction of China and its neighboring regions. In: Yin, A., Harrison, M. (Eds.), The Tectonic Evolution of Asia. Cambridge Univ. Press, New York, pp. 442–484.

Zhang, G.H., Zhou, X.H., Sun, M., Chen, S.H., Feng, J.L., 1998a. Highly chemical heterogeneity in the lower crust and crust–mantle transitional zone: geochemical evidences from xenoliths in Hannuoba basalt, Hebei province. Geochimica 27, 153–169 (in Chinese).

Zhang, G.H., Zhou, X.H., Sun, M., Chen, S.H., Feng, J.L., 1998b. Sr, Nd and Pb isotopic characteristics of granulite and pyroxenite xenoliths in Hannuoba basalts, Hebei province, and their implications for geologic processes. Acta Petrol. Sin. 14, 190–197 (in Chinese).

Zhi, X.C., Song, Y., Frey, F.A., Feng, J., Zhai, M., 1990. Geochemistry of Hannuoba basalts eastern China: constraints on the origin of continental alkali and tholeiitic basalts. Chem. Geol. 88, 1–33.

Zindler, A., Hart, S.R., 1986. Chemical geodynamics. Annu. Rev. Earth Planet. Sci. 14, 493–571.